Geomorphology 245 (2015) 223–230

Contents lists available at ScienceDirect

Geomorphology

journal homepage: www.elsevier.com/locate/geomorph

# Continuous monitoring bed-level dynamics on an intertidal flat: Introducing novel, stand-alone high-resolution SED-sensors

Zhan Hu [a,b], Walther Lenting [c], Daphne van der Wal [a], Tjeerd J. Bouma [a,*]

[a] Spatial Ecology Department, Royal Netherlands Institute for Sea Research, P.O. Box 140, 4400 AC Yerseke, The Netherlands
[b] Hydraulic Engineering Department, Delft University of Technology, P.O. Box 5048, 2600 GA Delft, The Netherlands
[c] Marine Technology Electronics Department, Royal Netherlands Institute for Sea Research, P.O. Box 59, 1790 AB Den Burg, Texel, The Netherlands

ARTICLE INFO

*Article history:*
Received 26 November 2014
Received in revised form 19 May 2015
Accepted 24 May 2015
Available online 27 May 2015

*Keywords:*
Sediment dynamics
Spatiotemporal scales
Hydrodynamic forcing
Measurement validation

ABSTRACT

Tidal flat morphology is continuously shaped by hydrodynamic forces, resulting in a highly dynamic bed surface. The knowledge of short-term bed-level changes is important both for assessing sediment transport processes as well as for understanding critical ecological processes, such as vegetation recruitment on tidal flats. High frequency bed-level measurements with a high vertical resolution are generally needed for hypothesis testing and numerical model validation. However, conventional manual bed-elevation measurements tend to have a coarse temporal resolution (weeks to months) due to the labor involved. Existing automated methods for continuous monitoring of bed-level changes either lack a high vertical resolution or are very expensive and therefore limited in spatial application. In light of this, we developed a novel instrument called SED (Surface Elevation Dynamics) sensor for continuous monitoring with a high vertical resolution (2 mm). This sensor makes use of light sensitive cells (i.e. phototransistors) and operates stand-alone. The unit cost and the labor in deployments are reduced, facilitating spatial application with a number of units. In this study, a group of SED-sensors is tested on a tidal flat in the Westerschelde Estuary, The Netherlands. The obtained bed-level changes are compared with the data obtained with precise manual measurements using traditional Sedimentation Erosion Bars (SEBs). An excellent agreement between the two methods was obtained, confirming the accuracy and precision of the SED-sensors. Furthermore, to demonstrate how the SED-sensors can be used for measuring short-term bed-level dynamics, two SED-sensors were deployed at two sites with contrasting wave exposure. Daily bed-level changes were obtained including a severe storm event. The difference in observed bed-level dynamics at both sites was statistically explained by their different hydrodynamic conditions. Thus, the stand-alone SED-sensor can be applied to monitor sediment surface dynamics with high vertical and temporal resolution, which provides opportunities to pinpoint morphological responses to various forces in intertidal environment. We expect that this sensor can also be applied in other morphological environments, such as rivers, salt-marsh, beaches and dunes, but the actual applicability remains to be tested. Furthermore, the SED-sensors may also offer opportunities for ground-truthing remote sensing techniques aimed at describing morphological changes. Finally, further improvements in future SED-sensors are discussed, including an inclination and compass sensor, wireless data retrieving function and additional IR-light bar for measurements with poor light availabilities.



## 1. Introduction

Tidal flats are commonly found in sediment-rich environments with gentle bed slopes (Friedrichs, 2011). Due to the absence of stabilizing vegetation cover, tidal flat topography is continuously shaped by hydrodynamic force from tidal currents and wind waves. As such force has great temporal and spatial variability on short time scales (i.e., hours to days), it may impose short-term surface-elevation dynamics (Le Hir et al., 2000; Green and Coco, 2014). The information of the short-term bed-level changes is important to pinpoint the effect of prevailing hydrodynamic forcing and understand fundamental processes in sediment transport (Friedrichs, 2011; Green and Coco, 2014). Moreover, the short-term dynamics of the tidal flat sediment surface is important for the recruitment of vegetation, microphytobenthos and benthic invertebrates (Bouma et al., 2001; Balke et al., 2011, 2014; Nambu et al., 2012; Fagherazzi et al., 2014), thereby influencing the ecosystem services delivered by tidal flats (Fagherazzi and Wiberg, 2009; Borsje et al., 2011; Foster et al., 2013; Temmerman et al., 2013; Bouma et al., 2014). High frequency bed-level measurements with a high vertical resolution are generally needed for hypothesis testing and numerical model validation in various biogeomorphological studies.

* Corresponding author.
*E-mail addresses:* zhan.hu@nioz.nl (Z. Hu), Walther.Lenting@nioz.nl (W. Lenting), Daphne.van.der.Wal@nioz.nl (D. van der Wal), Tjeerd.Bouma@nioz.nl (T.J. Bouma).

http://dx.doi.org/10.1016/j.geomorph.2015.05.027
0169-555X/

Conventional discontinuous surface-elevation monitoring typically has a coarse temporal resolution (weeks to months), determined by re-survey frequency (Lawler, 2008; Nolte et al., 2013). In tidal flat environments, the discontinuous methods include using erosion pins (Gabet, 1998; Stokes et al., 2010), Surface Elevation Table (SET, Cahoon et al., 2002), Sedimentation Erosion Bar (SEB, Van Wijnen and Bakker, 2001) and leveling (e.g. total station theodolite and differential GPS, Silva et al., 2013). Each method has its own advantages and disadvantages in terms of vertical resolution, ease and cost of covering multiple spots (Table 1). Nevertheless, none of these methods is suitable in continuously quantifying short-term (e.g. daily) surface elevation changes because of a prohibitively high cost of labor and traveling involved. Elevation can also be assessed with great spatial coverage, using for example airborne laser altimetry (LIDAR) techniques, photogrammetric and Structure from Motion (SfM) techniques (Millard et al., 2013; Fonstad et al., 2013; Mancini et al., 2013). Restricted overpass frequency and limited vertical resolution, however, make such methods less suitable for monitoring individual erosion and deposition events (Table 1).

To continuously measure sediment surface dynamics, a range of automated instruments have been developed over the years: the Photo-Electronic Erosion Pin (PEEP) sensor (Lawler, 1991), resistive rods (Ridd, 1992; Arnaud et al., 2009), and acoustic bed-level sensors (Andersen et al., 2006; Ganthy et al., 2013). Of these methods, the acoustic sensors, including ALTUS (Jestin et al., 1998; Ganthy et al., 2013), ADV (Acoustic Doppler Velocimeter (Andersen et al., 2006)) and PCADP (Pulse-Coherent Acoustic Doppler Profiler (Zhu et al., 2014)), generally have the highest vertical resolution (within 2 mm), but their application is typically relatively expensive (Table 1). Furthermore, most of these methods require alongside external power and data-logging systems, which leads to high unit cost and labor-intensive deployment. Monitoring at multiple disconnected locations to obtain spatial information is therefore restricted.

We designed a novel stand-alone instrument called SED (Surface Elevation Dynamics) sensor, in order to obtain a high vertical resolution at a reasonable cost. The SED-sensor detects sediment surface position by a dense array of light sensitive cells (i.e. phototransistors) placed as close as 2 mm apart, ensuring a high vertical resolution. Moreover, we supplied this SED-sensor with an internal data-logger and power supply, to enable stand-alone deployment. In this study, we aim to: (1) test the performance of this newly developed SED-sensor on an unvegetated, wave exposed intertidal flat; (2) demonstrate how the sensor can be used to measure surface-elevation dynamics with a high temporal (daily) and vertical resolution (2 mm) over a prolonged period of time; and (3) test if the observed bed-level dynamics can be related to physical forcing. To achieve these objectives, firstly, we deployed a set of 4 SED-sensors at a single location on a tidal flat, in the SW of Netherlands. The measured surface-elevation dynamics were compared with that obtained with a precise manual measurement: Sediment Erosion Bars (SEBs). Secondly, we use these SED-sensors to measure the daily surface-elevation dynamics on two contrasting sites during 1 month. The obtained bed level changes were interpreted in relation to the local tidal and wave conditions measured by alongside wave gauges.

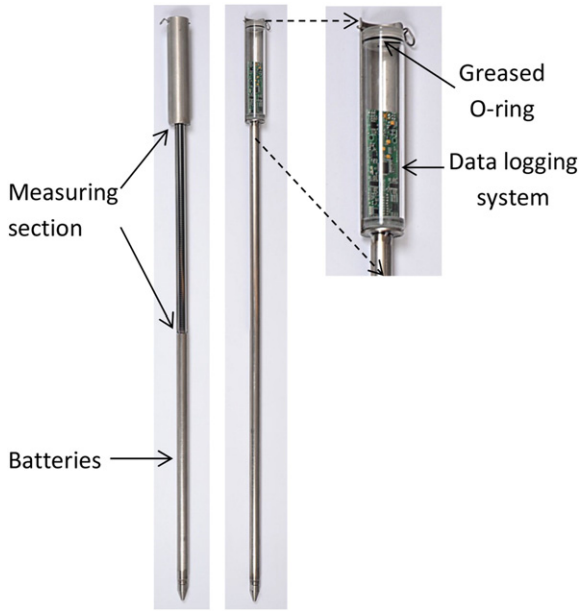


**Fig. 1.** Front side (left panel) and back side (middle panel) of the SED-sensor. The right panel is the enlarged data logging section of the sensor. The total length of the sensor is 1100 mm, and detailed dimensions are shown in Fig. 2.

**Table 1**
List of discontinuous and continuous methods used to measure bed-level changes.

| | Method | Reference (examples) | Estimated vertical resolution (mm) | Typical time resolution | Price range [a] (Euros) | Spatial coverage | Labor | Typical environments |
|---|---|---|---|---|---|---|---|---|
| Discontinuous method | SEB/SET | Cahoon et al. (2002), Van Wijnen and Bakker (2001) | 0.5–1.5 | Weeks–decades | <100 | Spot | High | Salt marshes, mangroves, tidal flats, subtidal areas |
| | Erosion pin | Gabet (1998), Stokes et al. (2010) | ~10 | Weeks–months | <5 | Spot | High | Salt marshes, mangroves, tidal flats, dunes, beaches |
| | Leveling | Silva et al. (2013) | 5–25 | Weeks–decades | <25,000 | ~1 km | High | Salt marshes, mangroves, tidal flats, dunes, beaches |
| | Ground-based LiDAR | Nagihara et al. 2004 | ~6 | Weeks–decades | <100,000 | ~0.3 $km^2$ | Medium | Salt marshes, mangroves, tidal flats, dunes, beaches |
| | Airborne LiDAR | Millard et al. (2013); Glenn et al., 2011 | 100–150 | Months–decades | <15,000 | >1 $km^2$ | Medium | Salt marshes, mangroves, tidal flats, dunes, beaches |
| | Photogrammetry/ SfM | Fonstad et al. (2013), Mancini et al. (2013) | 100–200 | Weeks–decades | <5000 | 0.1–1 $km^2$ | Medium | Tidal flats, dunes, beaches |
| Continuous method | SED sensor | This paper | 2 | Days–months | <1000 | Spot | Low | Salt marshes, mangroves, tidal flats, dunes, beaches |
| | PEEP | Lawler (1991, 2008) | ~2.3 [b] | Days–months | <1750 | Spot | Medium | River banks, gullies, canals, tidal mudbanks |
| | Electro-resistivity sensor | Ridd (1992), Arnaud et al. (2009) | 10–30 | Intra-tide–months | <6000 | Spot | Medium | Beaches |
| | Acoustic sensors | Jestin et al. (1998), Ganthy et al. (2013); | 1–2 | Intra-tide–months | <8000 | Spot | Medium | Salt marshes, tidal flats, dunes, beaches, subtidal areas |

[a] Prices are for a set of measuring and data logging instruments, based on quotes from corresponding manufactures. For methods that consist of different sets of devices (e.g. acoustic sensors includes ALTUS, ADV and PCADP), the listed price was from the method with lowest price. For airborne LiDAR, the price is based on one-time fly passage.
[b] This resolution was obtained in good natural light; it may be different in different light conditions because of the calibration and interpolation procedures.

## 2. Materials and methods

### 2.1. SED-sensor

The measuring section of a SED-sensor is a semi-continuous array of 200 light sensitive cells (Figs. 1, 2). The distance between two adjacent cells is 2 mm. Thus, the measuring section is ca. 400 mm long. The array of cells is packed in a transparent tube and is sealed at the top of the tube by a cap with a slightly greased O-ring to prevent water leakage. This kind of sealing is commonly used and very reliable in being watertight, provided that the cap is closed in a clean laboratory-environment. The whole tube is enclosed in a stainless sheath to increase its durability (Fig. 1). The sheath has a 400 mm-long window open on the front side of the sensor for measurement. The upper and lower part of the measuring section is the data logging and battery supply system of the SED-sensor respectively, which excludes the need for external data logger or power source.

When in use, a SED-sensor is inserted vertically into the seabed, leaving ca. half of the measuring section above the seabed (Fig. 2). Thus, the sensor has about 70 cm in total underground to ensure firmly standing in bed sediment. In environments with very soft bed materials or with violent hydrodynamic forcing, the underground length can be further increased to about 120 cm by connecting a 50 cm-long stainless metal extension at the end tip of the SED-sensor. If necessary, multiple extensions can be added to secure the sensor mounting. The sensor sheath has a sharp end tip (Fig. 1), which facilitates mounting the sensor to an adequate depth by gently pushing it down by hand. If the bed sediment is too hard to penetrate by manual pushing, one can make an initial hole (not deeper than the desired depth) in the sediment bed by hammering downward a wooden stick with a similar diameter as the SED-sensor. Subsequently, the SED-sensor can be pushed slowly into the hole until the desired mounting depth is achieved. The most of the sensor weight is from the stainless sheath of the sensor. To prevent the SED-senor being top-heavy and minimize any tendency towards inclination, the sheath is half-open at the head and the measuring section of the sensor, and it is fully closed at the lower part of the sensor. Additionally, batteries are also located near the bottom, adding considerable weight to the lower part of the sensor.

During measurement, a current runs through each light sensitive cell, which is proportional to the amount of light on each cell. This current is measured over a resistor to give a voltage output. In this way, above-ground and below-ground cells will give higher and lower output accordingly. Near the monitoring bed level, a transition point between low values to high values can be identified in the voltage output (Figs. 2, 3). It is noted that lights can penetrate vertically into the transparent tube and reach a few cells just below the bed level. Due to this light penetration, the transition from high to low voltage output does not occur exactly at the bed level. In order to minimize

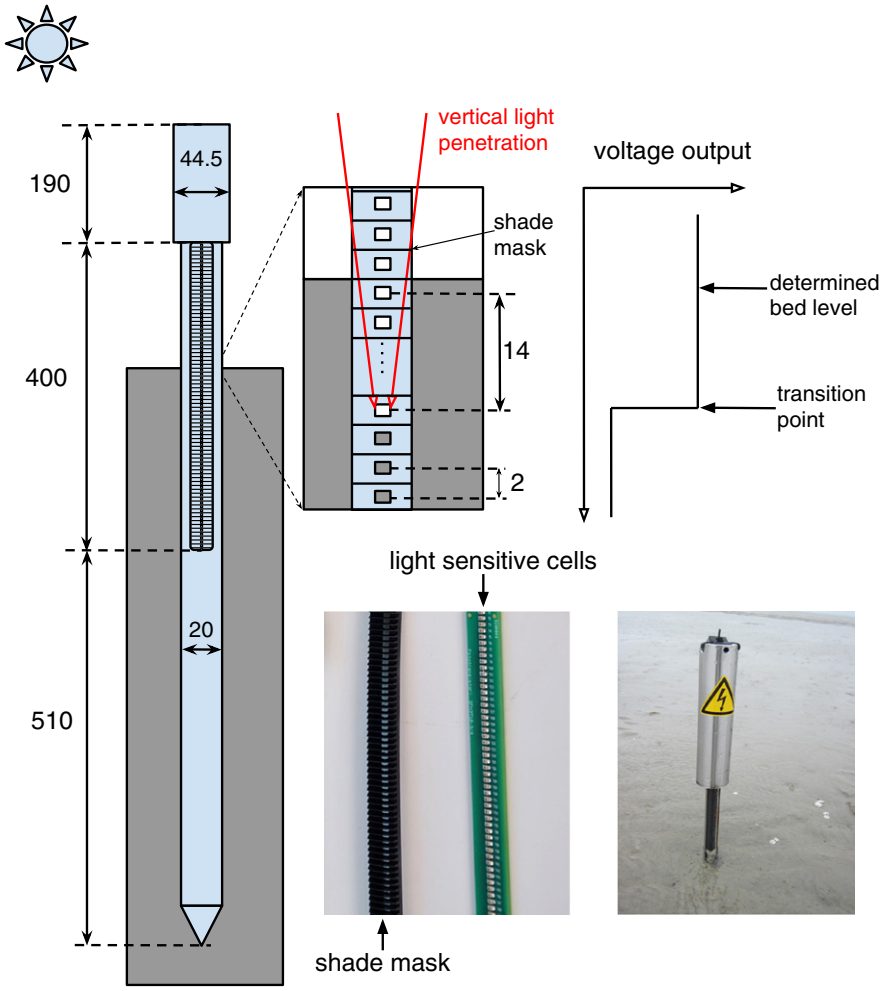


**Fig. 2.** Schematized of the SED-sensor in operation. Dimensions are in mm (not to scale). The individual light sensitive cell outputs voltages proportional to their light availability. The aboveground cells and belowground cells should give high and low outputs accordingly, resulting in a transition point at the bed level. However, light can penetrate vertically into the measuring section just below the bed level, which delays the transition point. A shade-mask that covers the light sensitive cells is placed to regulate such light penetration. Laboratory and field tests showed that with the shade-mask the distance between a transition point and the corresponding bed level was fixed to be 14 mm (i.e. 7 cells) in various light conditions. The lower two photos show the array of light sensitive cells, shade mask and SED-sensor deployed in field.

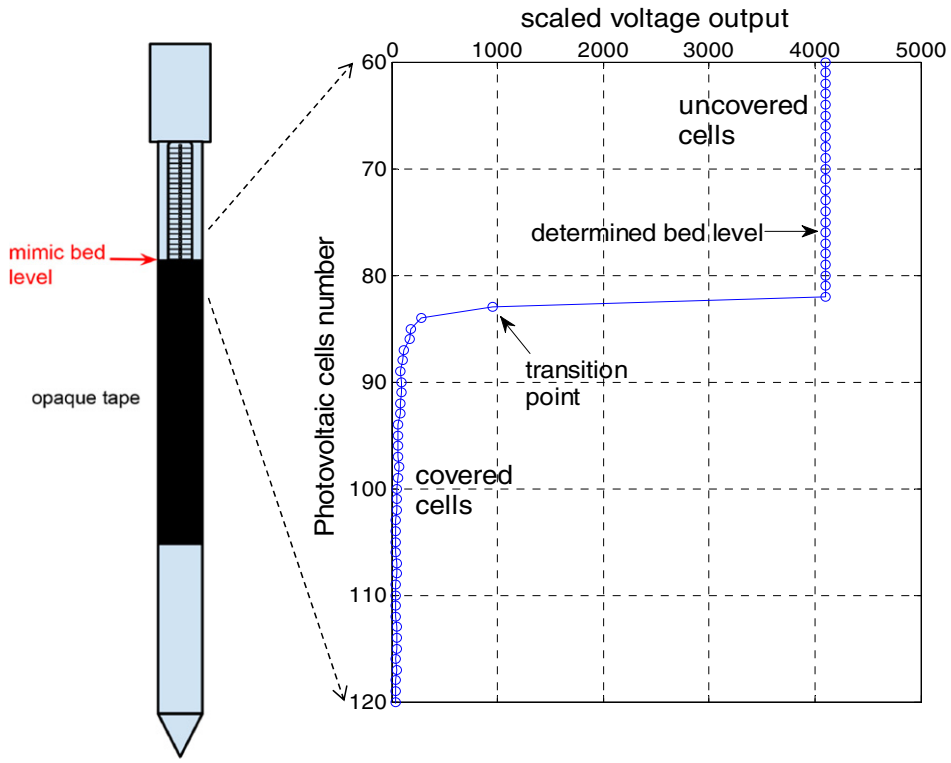


**Fig. 3.** Demonstration of how the bed-level can be determined by the SED-sensor, using the 'high sensitive' voltage output mode. The data shown was derived from a test carried out with a low-daylight intensity (15 μmol $m^{-2}$ $s^{-1}$). Part of the sensor was covered by opaque tape to mimic a fixed bed-level. The output of the uncovered cells is 4095, which is the maximum value that can be restored in 12 bits. The covered cells generally give a much lower voltage output. At the location of the transition point (i.e., going from the covered to uncovered cells), the voltage output difference between two adjacent cells is larger than 500. The mimicked bed level is 14 mm (i.e., 7 cells of 2 mm each) above the transition point. This distance of 14 mm is constant, regardless if ambient light levels are higher (data not shown). The shown data is from a part of the whole 200 photovoltaic cells array.

and regulate such vertical light penetration, we placed a customized shade-mask on the cells (Fig. 2).

As stated above, the current running through the light sensitive cells is transformed into a voltage over a resistor. By using resistors with high resistance ($10^6$ Ω), medium resistance ($10^4$ Ω) and low resistance ($10^2$ Ω), three different voltage outputs categorized as 'high sensitivity', 'medium sensitivity' and 'low sensitivity' are obtained in each measurement. For all the categories, the voltage measurement range is from 0 to 3.3 V and the outputs are scaled proportionally as integers between 0–4095 (unsigned 12-bit integers). In the 'high sensitivity' output, transition points can be detected even when the measurement is taken with a very low light intensity (e.g. 15 μmol $m^{-2}$ $s^{-1}$ in natural daylight, see Fig. 3). In this study, we use the 'high sensitivity' output to determine bed levels. The transition point (i.e. going from below-ground to above-ground cells) is determined as where the output difference between two adjacent cells is larger than a threshold value of 500 (corresponding to 0.40 V) (Fig. 3). With the shade-mask, the transition point is always, regardless of the light level, 14 mm (i.e. 7 cells) beneath the bed level (i.e., actual transition air to sediment). Such distance and threshold value for the transition point were determined by calibrating the sensor outputs against known bed-level positions (Fig. 3). For the calibration, we put opaque tape around the sensor to cover a part of its measuring section. The tape edge was then the mimicked bed-level, which is fixed over time. The calibration was done in varying light conditions both in laboratory and on a tidal flat (described in Section 2.2) over 3 days. In the field test, we assured the tape edge is well above the actual bed level, so that the mimicked bed level (i.e. tape edge) is constant in time and would not be affected by natural bed level fluctuations.

The measuring interval of the SED-sensor can be set from one second to a few hours, depending on the application. Because of an energy-saving design, even with a measuring interval as short as one minute, SED-sensors with 9 AAA batteries can continuously operate longer than 24 months. The voltage outputs from each interval are stored chronologically as a binary file in a microSD card. One-month deployment of the SED-sensor using one-minute interval only requires 70 MB storage room. Thus, a common microSD card with a memory capacity of 8 GB can provide sufficient storage for deployments last for months to years.

The SED-sensors rely on daylight, and hence do not work during night. When submerged by turbid water, a high sediment concentration layer may be present near the monitoring bed, which hinders determining the bed-level positions. Therefore, data acquired while the SED-sensor is submerged are excluded from analyses. In intertidal environments, the measuring window for the SED-sensors is then at low tide during daytime. The length of a measuring window depends on the local tidal condition and measuring elevation. The obtained bed-level dynamics is generally the overall change over one or two tidal cycles.

### 2.2. Comparing SED-sensor measurement with the SEB

In order to test the performance of the SED-sensor, we compared the SED-sensor measurements with Sediment Erosion Bar (SEB) measurements, a manual approach with an vertical resolution of 0.5 mm (Nolte et al., 2013) (Fig. 4). Four SED-sensors were placed at a same elevation (−0.61 m NAP — Normal Amsterdams Peil) on a tidal flat in the, in SW Netherlands. The Westerschelde is a meso to macrotidal estuary. The mean tide range is 4.1 m NAP at the study site and it is exposed to the wave actions induced by prevailing south-westerly winds (Callaghan et al., 2010). The distance between two adjacent SED-sensors was 1 m. Between two sensors, there was a PVC pole mounted for the SEB measurement (Fig. 4). To avoid possible disturbance of the seabed near the SED-sensors, the SEB measurements were carried out 50 mm left and right of the SED-sensor. The bed level was then determined by averaging the two readings.

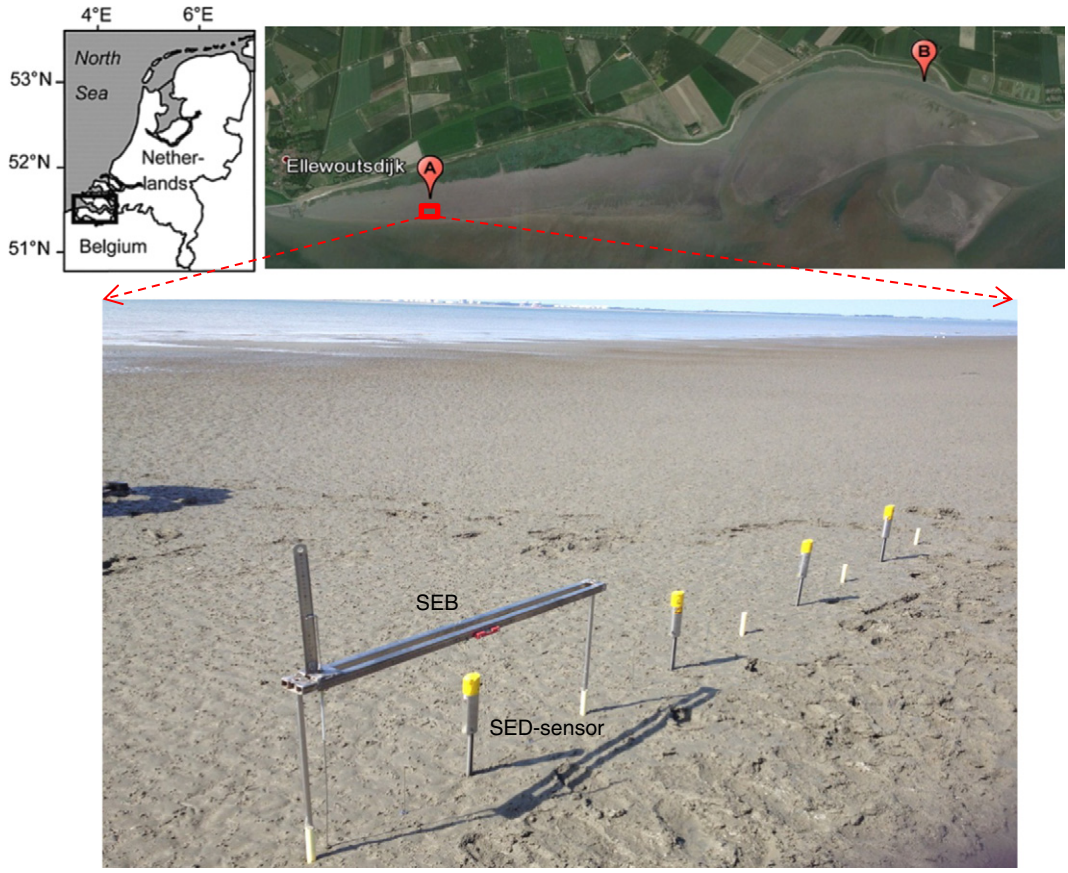


**Fig. 4.** Study site and sensor deployments. Top left panel, location of the Westerschelde in SW Netherlands; top right panel, the study site at a tidal flat near Ellewoutsdijk, image from Google Maps; the location of the SED-sensor test is indicated as a red square; 'A' and 'B' are the exposed and sheltered site where bed-level dynamics, tidal level and wave conditions were measured; bottom panel, deployments of SED-sensor and SEB comparison test.

The testing period was from 13 June 2014 through to 17 July 2014. SED-sensor measures the bed level dynamics continuously (every minute) during this period, whereas the measurement frequency of the manual SEB approach is limited by the frequency of field campaigns. In the testing period, six field SEB surveys were carried out on: 13 June 2014, 19 June 2014, 27 June 2014, 02 July 2014, 11 July 2014 and 17 July 2014. The SEB observations were done manually when the test location was emerged at low tide. The automatically recorded SED-sensor data in the same windows was used to compare with the SEB observations. In each window (2 h), there were 120 readings from each SED-sensor. Due the absence of hydrodynamic disturbance in these windows, the bed-level readings were expected to be constant. However, small reading variations may occur, depending on the water drainage condition on the bed surface. A small amount of water on the bed surface remains to be drained shortly after the receding tide, which can lead to different readings compared to the condition without any stagnant water. As the readings should be constant when the surface water is completely drained, we used the reading that had highest occurrence in a window as an effective SED-sensor measurement point. For both SED-sensor and SEB measurements, bed level changes were determined as the bed level difference between two consecutive surveys. Periods with net erosion were assigned negative values whereas periods with net sedimentation were assigned positive values.

### 2.3. Measuring surface-elevation dynamics and hydrodynamics at contrasting sites

To show how the SED-sensor can be used to obtain time series of short-term bed-level dynamics, two SED-sensors were placed at two sites, with similar elevations but contrasting wave exposure conditions (Fig. 4). The elevation of site A and B is 0.45 m NAP and 0.30 m NAP, respectively. The elevation difference (0.15 m) is considered small compared to the local tide range (4.1 m). Site A, on the western side of the tidal flat, is fully exposed to the wave force, whereas site B, on the eastern side of the tidal flat, is sheltered from waves because of the blockage of a seaward shoal (Callaghan et al., 2010). The measuring interval was also set to as short as 1 min to be able to capture short measuring windows. An effective bed-level monitoring point was determined as the readings with the highest occurrence in a window. The measurement period was 1 month, from 12 Oct 2013 through to 11 Nov 2013. The obtained bed-level time series is compared with the bed level measured at the initial deployment (as $t_0$). Based on the obtained bed-level time series, the overall dynamics of both sites can be assessed by the standard deviation of these data sets.

At each site, local tidal level and wave condition were measured by a pressure sensor (OSSI-010-003C; Ocean Sensor Systems, Inc.) deployed closed to the SED-sensor. The pressure sensor was placed 0.05 m above the seabed and the measuring frequency was 5 Hz. The measuring interval and the measuring period were 15 min and 7 min, respectively. Thus, 2100 data points were generated in each interval. The mean water level in an interval is determined by averaging all these data points. The wave analysis was based on pressure fluctuations. The attenuation of the pressure signals with water depth was corrected to derive bulk wave parameters, e.g. significant wave height ($H_s$) and peak wave period ($T_P$) (Tucker and Pitt, 2001).

To evaluate the relative importance of wave and tidal current forcing at different sites as driver of bed level dynamics, correlation coefficients between bed-level dynamics and corresponding hydrodynamic forcing

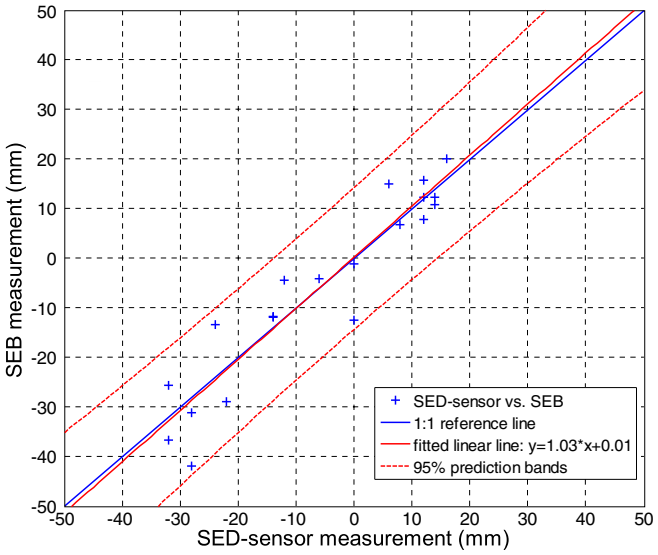


**Fig. 5.** Comparison of SED-sensor and SEB measurements; Positive and negative values represent sedimentation and erosion respectively.

were quantified. Specifically, the wave and tidal current forcing is represented by the maximum significant wave height ($H_s$) and peak tidal level in a tidal cycle. Peak tidal level provides a good proxy of maximum tidal current velocity (Bouma et al., 2005). In those cases that two consecutive bed-level observations integrate over two tidal cycles, the maximum $H_s$ and the maximum tidal level in these cycles selected for analysis.

## 3. Results

### 3.1. SED-sensor and SEB measurement comparison

Six field SEB surveys with four replicated measuring locations resulted in $(6-1)\times 4 = 20$ data points of surface elevation changes (Fig. 5). The same amount of SED-sensor data points was obtained using the readings with highest occurrence in corresponding measuring windows. On average, these readings have an occurrence of 57% in each window.

The obtained SED-sensor vs. SEB data points are very close to the 1:1 reference line, which shows a good agreement between SED-sensor and the precise manual SEB measurements. Using the data from the two methods, a fitted regression line can be obtained ($R^2 = 0.89$). The slope of the fitted line (1.03) is close to 1 and all the data points fall in the 95% prediction bands, which further confirms the consistency between the two measurements. This consistency also implies that scouring around the SED-sensor is limited due to the small sensor diameter (20 mm, see Fig. 2). Hence, it is not a problem for measuring the bed-level dynamics. We define the measurement accuracy as the absolute error between the SED-sensor result and the true value, which is assumed to be provided by the SEB measurement. Hence, based on all the data points (Fig. 5), the mean accuracy is estimated to be 5.0 mm with a standard deviation of 3.9 mm. The small difference between the two measurements is likely caused by the fact that these two instruments did not measure the exact same spots and small-scale sand ripples appeared on the bed surface (see Fig. 4). Notably, there was some biofilm developing on the SED-sensors during the testing period, but this fouling did not influence the observations with the 'high sensitivity' outputs.

### 3.2. Surface-elevation dynamics measured by the SED-sensors

In total, there were 41 effective bed-level monitoring points at site A over 59 tide cycles (Fig. 6). In the same period, there were 31 effective bed-level monitoring points at site B. For most cases (98%), there was at least one low-tide bed-level monitoring point per day. Thus, the bed-level monitoring at both sites generally provided the bed-level dynamics over one or two tide cycles. There were more monitoring points (measuring windows) at site A than site B due to its slightly higher elevation.

The obtained daily bed-level dynamics at two contrasting sites were interpreted in relation to the wave and tidal current forcing. At the two

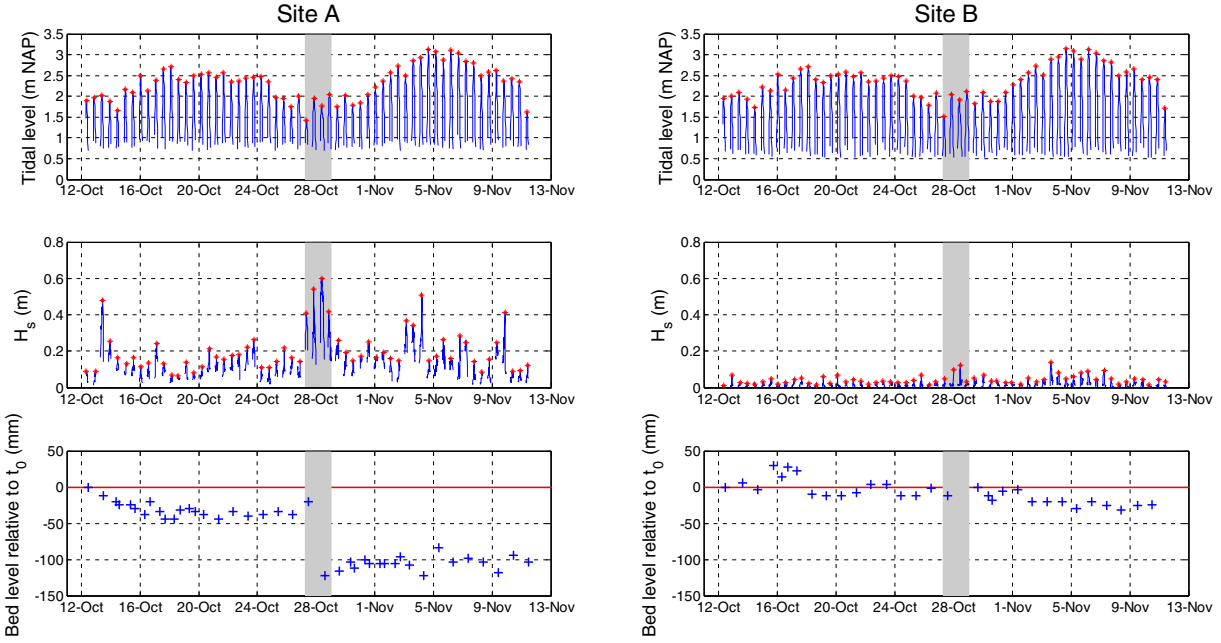


**Fig. 6.** Time-series of bed-level dynamics at sites A (exposed) and B (sheltered) in relation with the tidal level fluctuations and wave conditions. The red stars in the upper and the middle panels are the peak tidal elevation or peak signification wave height ($H_s$), respectively. The lower panels show the bed level relative to $t_0$ on 12 Oct 2013. Positive values indicate sedimentation, whereas negative values show erosion. The shaded area indicates a large storm event that occurred on 27 and 28 Oct 2013 (St. Jude storm).

**Table 2**
The correlation coefficient between bed-level changes and tidal current or wave forcing; '$p$' is the $p$-value for testing the hypothesis of no correlation, which is compared with a threshold equals to 0.05. The total number of data points from site A and site B is 41 and 31, respectively.

| | Site A | Site B |
|---|---|---|
| Tidal current forcing | $-0.26$ ($p = 0.10 > 0.05$) | $-0.45$ ($p = 0.01 < 0.05$) |
| Wave forcing | $-0.34$ ($p = 0.03 < 0.05$) | $-0.26$ ($p = 0.15 > 0.05$) |

sites, the tidal fluctuations are similar because of their similar elevations and the short distance between two locations. However, the wave conditions were significantly different (Fig. 6). The exposed site A had much higher $H_s$ than the sheltered site B, which leaded to more erosion (bottom panels in Fig. 6). Remarkably, during St. Jude storm on 27 and 28 Oct 2013, severe erosion was observed at site A. Bed level was lowered as much as 102 mm in two tidal cycles. However, no significant erosion is observed at the site B following the storm, as the seaward shoal greatly attenuated the incident wave height (middle panels in Fig. 6).

In order to evaluate the relative importance of tidal and wave forcing, correlation coefficients between the bed-level changes and the corresponding hydrodynamic forcing was quantified (Table 2). They indicate that the bed level dynamics at the exposed site A is significantly correlated with its wave forcing ($p < 0.05$), whereas the sheltered site B is significantly correlated with the tidal forcing ($p < 0.05$). Therefore, bed-level dynamics at site A and B is primarily related to wave forcing and tidal current forcing, respectively. The correlation coefficients are negative, suggesting that stronger corresponding hydrodynamic force leads to higher erosion in the observed bed levels. Furthermore, the overall bed-level dynamics at these two sites can be assessed by the standard deviations. For site A and B, the standard deviation is 39 mm and 17 mm, respectively. Thus, the exposed site A has higher bed-level variations than site B.

## 4. Discussion

A good agreement between the SED-sensor and the SEB measurements is obtained in the SED-sensor performance test. The operational accuracy of the SED-sensor is estimated to be 5.0 mm with a 3.9 mm standard deviation based on the comparison of the two methods. The SEB is a classical high-accuracy bed-level monitoring method with an mm-scale resolution (Van Duin et al., 1997; Van Wijnen and Bakker, 2001; Nolte et al., 2013). Hence, the good agreement between both methods implies that the SED-sensor is a reliable method to provide accurate high-resolution bed-level change data. As bed levels can be detected with low light intensity using the 'high sensitivity' output of the SED-sensor, the measurement accuracy is not influenced by the varying light condition during daytime or some fouling on the SED-sensors. However, for long deployments covering several months, the SED-sensors may require regular cleaning to prevent excessive fouling.

The frequent monitoring of bed level elevation with the SED-sensor, enables pinpointing the effect of specific hydrodynamic forcing on the tidal flat morphology (Fig. 6). In rare occasions, the same temporal resolution was obtained using SEB, which reveals highly interesting bed-level dynamics (Yang et al., 2008). Nevertheless, the automated SED-sensor can general offer much higher temporal resolution than that typically obtained from conventional discontinuous measuring methods such as SEB and erosion pins (Van Wijnen and Bakker, 2001; Lawler, 2008). As SED-sensors do not measure in nocturnal or submerged conditions, the effective monitoring frequency in intertidal environments is related to the emersion duration, as well as the selected frequency of measurement. As in our study, this will generally provide sufficient measuring windows to observe the short-term bed-level dynamics and relate it to the prevailing hydrodynamic forcing condition. To enable monitoring in nocturnal and submerged conditions, we have started testing second version SED-sensors with an additional IR-light bar that enlightens the light-sensitive cells during each measurement. Furthermore, to leave the SED-sensor unmoved for prolonged time, data can be extracted wirelessly in-situ in future with the second version SED-sensor.

In our field measurements, the inclination angle between the SED-sensor and the vertical is negligible, causing limited effect on the bed-level measurement. However, the inclination angle can be larger in other situations. Especially in the environments with soft bed substance, the inclination angle may also vary slightly during events with strong hydrodynamic forces. It is then useful to include additional inclination angle measurement in order to record the sensor movement during extreme conditions and to correct the corresponding bed-level measurement. Similar to the ARGUS surface meter (ASM) system (Svenson et al., 2011; Vijverberg et al., 2011), the second version of the SED-sensor contains a LSM303DLHC 3D force and 3D compass sensor. The data from this LSM303DLHC sensor is stored for each measurement, so that a correction for inclination of the sensor per measurement will be implemented in future measurements.

Besides bare tidal flats, SED-sensors may also be used to measure the bed level changes in a number of other intertidal and subaerial environments. For example, these sensors are expected to be applicable in salt-marsh and mangroves since the light-reduction by shading from vegetation is likely to be too little to affect the monitoring, whereas other methods (e.g. SfM) may have difficulties in determining bed-level in vegetated areas (Fonstad et al., 2013). Furthermore, since the SED-sensors can be deployed over a prolonged period, they can also be inserted horizontally into the salt-marsh cliff to monitor its rate of retreat. Lastly, the measuring interval of SED-sensors can be set as short as 1 s, which offers an opportunity to monitor very rapid processes, e.g., aeolian transport on beaches and dunes. The actual applicability of this sensor in other environments (e.g. salt-marsh, rivers, beaches and dunes) remains to be tested. Overall, the SED-sensors may also offer a useful ground-truthing method for rapidly developing remote sensing techniques aimed at describing morphological changes.

## 5. Conclusions

Results of this study show that the newly developed SED-sensors can accurately monitor short-term bed-level changes originated from sediment erosion and deposition events. The SED-sensor measurement showed an excellent agreement with the most precise manual measurements such as Sediment Erosion Bars (SEBs). An operational accuracy as high as 5.0 mm (with standard deviation being 3.9 mm) is obtained from the comparison with the SEB measurement. Furthermore, the time series of bed-level dynamics obtained by using SED-sensors revealed contrasting characteristics at different sites, which could be explained by the contrasting hydrodynamic forcing. While further monitoring is needed to fully reveal the spatial and temporal variability of tidal flat sediment dynamics, our results suggest that the novel stand-alone high-resolution SED-sensor provide a reliable method to monitor bed-level dynamics in a number of environments. The major advantages of the SED-sensors are: (1) high vertical resolution monitoring ensured by a dense array of light sensitive cells; (2) suitable for automated continuous long-term monitoring in the intertidal and other environments; and (3) stand-alone design with internal power and data-logging systems that reduce the unit cost and deployment labor in large-scale monitoring.

## Acknowledgments

This study has been supported by Technology Foundation STW (project number: 07324/BEB. 7324), Rijkswaterstaat (project number: 4500220328) and EU FAST (grant agreement 607131). The first author (Z. Hu) is supported by the China Scholarship Council (grant number: 2010671012). We thank Qin Zhu, Martijn Henriquez, Sierd de Vries, Hervé Jestin and Mathieu Cassen for providing information in Table 1.

We specially thank Lennart van IJzerloo, Jeroen van Dalen, Jianfeng Tao and Xianye Wang for their help with field works.

## References


Andersen, T.J., Pejrup, M., Nielsen, A.A., 2006. Long-term and high-resolution measurements of bed level changes in a temperate, microtidal coastal lagoon. Mar. Geol. 226, 115–125. http://dx.doi.org/10.1016/j.margeo.2005.09.016.

Arnaud, G., Mory, M., Abadie, S., Cassen, M., 2009. Use of a resistive rods network to monitor bathymetric evolution in the surf/swash zone. J. Coast. Res. 1781–1785.

Balke, T., Bouma, T.J., Horstman, E.M., Webb, E.L., Erftemeijer, P.L.A., Herman, P.M.J., 2011. Windows of opportunity: thresholds to mangrove seedling establishment on tidal flats. Mar. Ecol. Prog. Ser. 440, 1–9.

Balke, T., Herman, P.M.J., Bouma, T.J., 2014. Critical Transitions in Disturbance-driven Ecosystems: Identifying Windows of Opportunity for Recovery.

Borsje, B.W., van Wesenbeeck, B.K., Dekker, F., Paalvast, P., Bouma, T.J., van Katwijk, M.M., de Vries, M.B., 2011. How ecological engineering can serve in coastal protection. Ecol. Eng. 37, 113–122.

Bouma, H., Duiker, J.M.C., De Vries, P.P., Herman, P.M.J., Wolff, W.J., 2001. Spatial pattern of early recruitment of *Macoma balthica* (L.) and *Cerastoderma edule* (L.) in relation to sediment dynamics on a highly dynamic intertidal sandflat. J. Sea Res. 45, 79–93. http://dx.doi.org/10.1016/S1385-1101(01)00054-5.

Bouma, T.J., De Vries, M.B., Low, E., Kusters, L., Herman, P.M.J., Tánczos, I.C., Temmerman, S., Hesselink, A., Meire, P., Van Regenmortel, S., 2005. Flow hydrodynamics on a mudflat and in salt marsh vegetation: identifying general relationships for habitat characterisations. Hydrobiologia 540, 259–274.

Bouma, T.J., van Belzen, J., Balke, T., Zhu, Z., Airoldi, L., Blight, A.J., Davies, A.J., Galvan, C., Hawkins, S.J., Hoggart, S.P.G., Lara, J.L., Losada, I.J., Maza, M., Ondiviela, B., Skov, M.W., Strain, E.M., Thompson, R.C., Yang, S., Zanuttigh, B., Zhang, L., Herman, P.M.J., 2014. Identifying knowledge gaps hampering application of intertidal habitats in coastal protection: opportunities & steps to take. Coast. Eng. 87, 147–157. http://dx.doi.org/10.1016/j.coastaleng.2013.11.014.

Cahoon, D.R., Lynch, J.C., Hensel, P., Boumans, R., Perez, B.C., Segura, B., Day Jr., J.W., 2002. High-precision measurements of wetland sediment elevation: I. Recent improvements to the sedimentation–erosion table. J. Sediment. Res. 72, 730–733. http://dx.doi.org/10.1306/020702720730.

Callaghan, D.P., Bouma, T.J., Klaassen, P., van der Wal, D., Stive, M.J.F., Herman, P.M.J., 2010. Hydrodynamic forcing on salt-marsh development: distinguishing the relative importance of waves and tidal flows. Estuar. Coast. Shelf Sci. 89, 73–88.

Fagherazzi, S., Wiberg, P.L., 2009. Importance of wind conditions, fetch, and water levels on wave-generated shear stresses in shallow intertidal basins. J. Geophys. Res. B: Solid Earth 114.

Fagherazzi, S., Mariotti, G., Banks, A.T., Morgan, E.J., Fulweiler, R.W., 2014. The relationships among hydrodynamics, sediment distribution, and chlorophyll in a mesotidal estuary. Estuar. Coast. Shelf Sci. 144, 54–64. http://dx.doi.org/10.1016/j.ecss.2014.04.003.

Fonstad, M.A., Dietrich, J.T., Courville, B.C., Jensen, J.L., Carbonneau, P.E., 2013. Topographic structure from motion: a new development in photogrammetric measurement. Earth Surf. Process. Landf. 38, 421–430. http://dx.doi.org/10.1002/esp.3366.

Foster, N.M., Hudson, M.D., Bray, S., Nicholls, R.J., 2013. Intertidal mudflat and saltmarsh conservation and sustainable use in the UK: a review. J. Environ. Manag. 126, 96–104. http://dx.doi.org/10.1016/j.jenvman.2013.04.015.

Friedrichs, C.T., 2011. Tidal Flat Morphodynamics: A Synthesis. In: Wolanski, E., McLusky, D. (Eds.), Treatise on Estuarine and Coastal Science. Academic Press, Waltham, pp. 137–170.

Gabet, E.J., 1998. Lateral migration and bank erosion in a saltmarsh tidal channel in San Francisco Bay, California. Estuaries 21, 745–753. http://dx.doi.org/10.2307/1353278.

Ganthy, F., Sottolichio, A., Verney, R., 2013. Seasonal modification of tidal flat sediment dynamics by seagrass meadows of *Zostera noltii* (Bassin d'Arcachon, France). J. Mar. Syst. S233–S240 http://dx.doi.org/10.1016/j.jmarsys.2011.11.027 (XII International Symposium on Oceanography of the Bay of Biscay 109–110, Supplement).

Glenn, N.F., Spaete, L.P., Sankey, T.T., Derryberry, D.R., Hardegree, S.P., Mitchell, J., 2011. Errors in LiDAR-derived shrub height and crown area on sloped terrain. J. Arid Environ. 75, 377–382. http://dx.doi.org/10.1016/j.jaridenv.2010.11.005.

Green, M.O., Coco, G., 2014. Review of wave-driven sediment resuspension and transport in estuaries. Rev. Geophys. 52, 77–117. http://dx.doi.org/10.1002/2013RG000437.

Jestin, H., Bassoullet, P., Le Hir, P., L'Yavanc, J., Degres, Y., 1998. Development of ALTUS, a high frequency acoustic submersible recording altimeter to accurately monitor bed elevation and quantify deposition or erosion of sediments. OCEANS '98 Conference Proceedings. Presented at the OCEANS '98 Conference Proceedings. vol. 1, pp. 189–194. http://dx.doi.org/10.1109/OCEANS.1998.725734.

Lawler, D.M., 1991. A new technique for the automatic monitoring of erosion and deposition rates. Water Resour. Res. 27, 2125–2128. http://dx.doi.org/10.1029/91WR01191.

Lawler, D.M., 2008. Advances in the continuous monitoring of erosion and deposition dynamics: developments and applications of the new PEEP-3T system. Geomorphology 93, 17–39. http://dx.doi.org/10.1016/j.geomorph.2006.12.016.

Le Hir, P., Roberts, W., Cazaillet, O., Christie, M., Bassoullet, P., Bacher, C., 2000. Characterization of intertidal flat hydrodynamics. Cont. Shelf Res. 20, 1433–1459.

Mancini, F., Dubbini, M., Gattelli, M., Stecchi, F., Fabbri, S., Gabbianelli, G., 2013. Using unmanned aerial vehicles (UAV) for high-resolution reconstruction of topography: the structure from motion approach on coastal environments. Remote Sens. 5, 6880–6898. http://dx.doi.org/10.3390/rs5126880.

Millard, K., Redden, A.M., Webster, T., Stewart, H., 2013. Use of GIS and high resolution LiDAR in salt marsh restoration site suitability assessments in the upper Bay of Fundy, Canada. Wetl. Ecol. Manag. 21, 243–262. http://dx.doi.org/10.1007/s11273-013-9303-9.

Nagihara, S., Mulligan, K.R., Xiong, W., 2004. Use of a three-dimensional laser scanner to digitally capture the topography of sand dunes in high spatial resolution. Earth Surf. Process. Landf. 29, 391–398. http://dx.doi.org/10.1002/esp.1026.

Nambu, R., Saito, H., Tanaka, Y., Higano, J., Kuwahara, H., 2012. Wave actions and topography determine the small-scale spatial distribution of newly settled Asari clams *Ruditapes philippinarum* on a tidal flat. Estuar. Coast. Shelf Sci. 99, 1–9.

Nolte, S., Koppenaal, E.C., Esselink, P., Dijkema, K.S., Schuerch, M., De Groot, A.V., Bakker, J.P., Temmerman, S., 2013. Measuring sedimentation in tidal marshes: a review on methods and their applicability in biogeomorphological studies. J. Coast. Conserv. 17, 301–325. http://dx.doi.org/10.1007/s11852-013-0238-3.

Ridd, P.V., 1992. A sediment level sensor for erosion and siltation detection. Estuar. Coast. Shelf Sci. 35, 353–362.

Silva, T.A., Freitas, M.C., Andrade, C., Taborda, R., Freire, P., Schmidt, S., Antunes, C., 2013. Geomorphological response of the salt-marshes in the Tagus estuary to sea level rise. J. Coast. Res. 582–587 http://dx.doi.org/10.2112/SI65-099.

Stokes, D.J., Healy, T.R., Cooke, P.J., 2010. Expansion dynamics of monospecific, temperate mangroves and sedimentation in two embayments of a barrier-enclosed lagoon, Tauranga Harbour, New Zealand. J. Coast. Res. 113–122 http://dx.doi.org/10.2112/08-1043.1.

Svenson, C., Gehres, N., Winterscheid, A., 2011. A high resolution optical backscatter survey in the Lower Elbe — deductions for near-bed suspended sediment transport in a meso-tidal environment. J. Coast. Res. 1599–1603.

Temmerman, S., Meire, P., Bouma, T.J., Herman, P.M.J., Ysebaert, T., De Vriend, H.J., 2013. Ecosystem-based coastal defence in the face of global change. Nature 504, 79–83. http://dx.doi.org/10.1038/nature12859.

Tucker, M.J., Pitt, E.G., 2001. Waves in Ocean Engineering. 1 ed. Elsevier Science, Oxford, UK.

Van Duin, W.E., Dijkema, K.S., Zegers, J., 1997. Veranderingen in bodemhoogte (opslibbing, erosie en inklink) in de Peazemerlannen. IBN-report 326, Wageningen.

Van Wijnen, H.J., Bakker, J.P., 2001. Long-term surface elevation change in salt marshes: a prediction of marsh response to future sea-level rise. Estuar. Coast. Shelf Sci. 52, 381–390. http://dx.doi.org/10.1006/ecss.2000.0744.

Vijverberg, T., Winterwerp, J.C., Aarninkhof, S.G.J., Drost, H., 2011. Fine sediment dynamics in a shallow lake and implication for design of hydraulic works. Ocean Dyn. 61, 187–202. http://dx.doi.org/10.1007/s10236-010-0322-2.

Yang, S.L., Li, H., Ysebaert, T., Bouma, T.J., Zhang, W.X., Wang, Y.Y., Li, P., Li, M., Ding, P.X., 2008. Spatial and temporal variations in sediment grain size in tidal wetlands, Yangtze Delta: on the role of physical and biotic controls. Estuar. Coast. Shelf Sci. 77, 657–671.

Zhu, Q., Yang, S.L., Ma, Y., 2014. Intra-tidal sedimentary processes associated with combined wave–current action on an exposed, erosional mudflat, southeastern Yangtze River Delta, China. Mar. Geol. 347, 95–106. http://dx.doi.org/10.1016/j.margeo.2013.11.005.